polymers

MDPI

Article

Nanomicelles of Radium Dichloride [^{223}Ra]$RaCl_2$ Co-Loaded with Radioactive Gold [^{198}Au]Au Nanoparticles for Targeted Alpha–Beta Radionuclide Therapy of Osteosarcoma

Bárbara Nayane Rosário Fernandes Souza [1], Elisabete Regina Fernandes Ramos Ribeiro [1], Aline Oliveira da Silva de Barros [1], Martha Sahylí Ortega Pijeira [1], Hericka Oliveira Kenup-Hernandes [2], Eduardo Ricci-Junior [3], Joel Félix Silva Diniz Filho [4], Clenilton Costa dos Santos [4], Luciana Magalhães Rebelo Alencar [4], Mohamed F. Attia [5], Sara Gemini-Piperni [6] and Ralph Santos-Oliveira [1,7,*]

1 Argonauta Nuclear Reactor Center, Nuclear Engineering Institute, Brazilian Nuclear Energy Commission, Rio de Janeiro 21941-906, Brazil; babinayane@gmail.com (B.N.R.F.S.); betebergmaria@gmail.com (E.R.F.R.R.); alinedbcg@gmail.com (A.O.d.S.d.B.); msopijeira@gmail.com (M.S.O.P.)
2 Laboratory of Nanoradiopharmaceuticals and Synthesis of Novel Radiopharmaceuticals, Nuclear Engineering Institute, Brazilian Nuclear Energy Commission, Rio de Janeiro 21941-906, Brazil; hkenup@ien.gov.br
3 DEFARMED Laboratory, Faculdade de Farmácia, Universidade Federal do Rio de Janeiro, Rio de Janeiro 21941-900, Brazil; ricci@pharma.ufrj.br
4 Laboratory of Biophysics and Nanosystems, Department of Physics, Federal University of Maranhão, São Luís 65080-805, Brazil; joelfelixdiniz@gmail.com (J.F.S.D.F.); cleniltoncs@gmail.com (C.C.d.S.); lucianamagal@gmail.com (L.M.R.A.)
5 Center for Nanotechnology in Drug Delivery, Eshelman School of Pharmacy, Division of Pharmacoengineering and Molecular Pharmaceutics, University of North Carolina at Chapel Hill, Chapel Hill, NC 27599, USA; mattia@email.unc.edu
6 Instituto de Ciências Biomédicas, Universidade Federal do Rio de Janeiro, Rio de Janeiro 21941-902, Brazil; sara.gemini@hotmail.com
7 Laboratory of Radiopharmacy and Nanoradiopharmaceuticals, Zona Oeste State University, Rio de Janeiro 23070-200, Brazil
* Correspondence: presidenciaradiofarmacia@gmail.com

check for updates

Citation: Souza, B.N.R.F.; Ribeiro, E.R.F.R.; da Silva de Barros, A.O.; Pijeira, M.S.O.; Kenup-Hernandes, H.O.; Ricci-Junior, E.; Diniz Filho, J.F.S.; dos Santos, C.C.; Alencar, L.M.R.; Attia, M.F.; et al. Nanomicelles of Radium Dichloride [^{223}Ra]$RaCl_2$ Co-Loaded with Radioactive Gold [^{198}Au]Au Nanoparticles for Targeted Alpha–Beta Radionuclide Therapy of Osteosarcoma. *Polymers* **2022**, *14*, 1405. https://doi.org/10.3390/polym14071405

Academic Editor: Dimitrios Bikiaris

Received: 13 March 2022
Accepted: 26 March 2022
Published: 30 March 2022

Publisher's Note: MDPI stays neutral with regard to jurisdictional claims in published maps and institutional affiliations.

Abstract: Alpha and beta particulate radiation are used for non-treated neoplasia, due to their ability to reach and remain in tumor sites. Radium-223 (^{223}Ra), an alpha emitter, promotes localized cytotoxic effects, while radioactive gold (^{198}Au), beta-type energy, reduces radiation in the surrounding tissues. Nanotechnology, including several radioactive nanoparticles, can be safely and effectively used in cancer treatment. In this context, this study aims to analyze the antitumoral effects of [^{223}Ra]Ra nanomicelles co-loaded with radioactive gold nanoparticles ([^{198}Au]AuNPs). For this, we synthesize and characterize nanomicelles, as well as analyze some parameters, such as particle size, radioactivity emission, dynamic light scattering, and microscopic atomic force. [^{223}Ra]Ra nanomicelles co-loaded with [^{198}Au]AuNPs, with simultaneous alpha and beta emission, showed no instability, a mean particle size of 296 nm, and a PDI of 0.201 (±0.096). Furthermore, nanomicelles were tested in an in vitro cytotoxicity assay. We observed a significant increase in tumor cell death using combined alpha and beta therapy in the same formulation, compared with these components used alone. Together, these results show, for the first time, an efficient association between alpha and beta therapies, which could become a promising tool in the control of tumor progression.

Keywords: alpha–beta therapy; bone cancer; radium-223 dichloride; radioactive gold nanoparticles; nanomicelles

1. Introduction

Targeted radionuclide therapy consists of a modality of treatment in which a biological effect is obtained by the energy absorbed from the radiation emitted by the radionuclide.

Targeted radionuclide therapy is an optimal choice for intractable tumors [1]. There are the following three types of particulate radiation used for targeted radionuclide therapy: (i) alpha particles, (ii) beta particles, and (iii) Auger electrons. According to Ersahin et al. [2], radionuclides that emit α- or β-particles are preferred for the treatment of bulky tumors. At the same time, Auger electrons can be used for small clusters of cancer cells or small tumor deposits. For therapeutic purposes, radiations with high linear energy transfer (LET), such as α- and β-particles, are preferable [3].

The efficacy of systemic or localized cancer therapy rests on the ability of the radionuclide to reach and remain in the tumor site specifically. In this regard, to increase the targeting and efficacy of radionuclide therapy, the use of these radionuclides, inserted into nanoplatforms, may represent an innovative and effective approach, since nanoparticles (NPs) may (i) improve the bioavailability, (ii) increase the biological half-life, and (iii) increase the targeting of the drug to a specific location [4–8].

^{198}Au is a beta-emitting radioisotope that has attracted interest in cancer molecular therapy using radioactive nanoparticles [9]. The mean penetration range (0.38 mm) in the tissue of beta particles of ^{198}Au (0.960 MeV_{max}) is sufficient to destroy tumor cells [10]. The beta particles have less energy than alpha particles; consequently, they cause less cytotoxicity. However, they can travel longer distances in circulation and damage DNA, promoting tumor cell death [11,12]. Moreover, ^{198}Au has an appropriate half-life (2.7 d) for clinical application [10]. Thus, the conversion of ^{198}Au into [^{198}Au]AuNPs is an attractive option, due to its ability to produce varying forms and sizes, enabling direct delivery to the cancer site [13,14].

During the last decades, gold nanoparticles (AuNPs) have exhibited promissory potential for the diagnosis of various cancers and treatment, owing to their morphological and structural nature, surface chemical modification, and tunable sizes and shapes [15–21]. Gold is considered the most stable nanoparticle and the most common among noble metals [22,23]. It has low cytotoxicity compared to other metals, high targeting ability, well-established synthesis, easy surface functionalization, and high bio-interaction with target cells, and is non-immunogenic [16,22,24–30]. Furthermore, AuNPs can be prepared in different shapes, such as sticks, cages, and spheres, with sizes ranging from 1 nm to over 100 nm [31]. Conversely, [^{198}Au]AuNPs are of increasing interest for local radionuclide therapy, as a powerful alternative for cancer treatment [15,32–35]. Several reports have shown the excellent efficacy of [^{198}Au]AuNPs for tumor shrinkage in vivo [14,36–38]. Furthermore, [^{198}Au]AuNPs have the advantage of being nanosized radioactive particles, with the potential to contain several radioactive atoms in a single particle [39,40].

On the other hand, ^{223}Ra is an alpha emitter radionuclide that emits high-energy alpha particles (95.3% (energy range of 5.0–7.5 MeV)) of short range (<100 μm/10 μm cell diameters) [41–44], which endows short penetration, promoting localized cytotoxic effects, with shallow toxic effects on the adjacent healthy tissue [45–47]. In addition, it is a radionuclide with a suitable half-life (11.4 d) for clinical application [19,48]. The ^{223}Ra acts as a calcium mimetic drug, predominantly accumulating in the bone tissues of the body [48,49]. In fact, ^{223}Ra is currently used in targeted alpha therapy (TAT) for treating bone metastases of patients with metastatic castration-resistant prostate cancer [50]. For this, ^{223}Ra is used in the chemical form of the salt radium dichloride ([^{223}Ra]$RaCl_2$). However, the preparation of stable formulations of ^{223}Ra is challenging because of the daughter isotopes' recoil energy and different chemical properties [51]. Although there are carriers reported for ^{223}Ra, such as liposomes [52], iron oxide [53], hydroxyapatite particles [54], etc., there is still a problem in the radionuclide formulation for generating a stable product, with targeted distribution to organs and tissues [48]. In this sense, the use of 127-Pluronic nanomicelles works as an alternative to solve this problem.

Nanomicelles are well known as excellent drug delivery systems; they have structural stability, nanoscale size, and low cytotoxicity, and they minimize drug degradation, reduce adverse side effects, and improve drug bioavailability [55,56]. Nanomicelles are colloidal structures (5–100 nm), formed from amphiphilic monomers, with a hydrophilic outer layer

and a hydrophobic inner layer. Due to their amphiphilic nature, normal nanomicelles encapsulate hydrophobic drugs and aid in their delivery. In the case of reverse nanomicelles, they can be used to encapsulate hydrophilic drugs, acting as better candidates for their delivery [57,58]. However, only a few works have reported the use of nanomicelles for the delivery of therapeutic radionuclides. These radionuclides were yttrium-90 and iodine-131 [59,60], which decay by the emission of beta particles. Thus, there are a lack of nanomicelles radiolabeled with alpha radionuclides, such as ^{223}Ra.

Recently, our group developed 127-Pluronic-[^{223}Ra]$RaCl_2$ nanomicelles, which showed dose–response behavior and an increased effect on osteosarcoma cells, decreasing the cell viability more efficiently [61]. Pluronic F127 is a poly(ethylene oxide)–poly(propylene oxide)–poly(ethylene oxide) (PEO–PPO–PEO) copolymer, which forms micelles with the PPO as a hydrophobic core and the terminal PEO segment acting as a hydrophilic corona [62–64]. Polymeric micelles, such as Pluronic®, have often been employed for sustained release, achieving an extended circulation time, favorable biodistribution, reduced side effects, and lower toxicity [55,65]. Nanomicelles, compared with conventional micelles, are more thermodynamically stable in physiological solutions [57]. Moreover, nanomicelles show some advantages, due to their great biocompatibility, simple preparation methods, effectiveness, and low cost [66].

Therefore, the need to modernize antitumor therapies has led to nanotechnology aiming to develop a more effective, safe, and efficient therapy. In this sense, radioactive nanoparticles have gained attention, due to their physical-chemical characteristics, biocompatibility, low toxicity, bioconjugation, and few side effects for healthy cells [67–69]. Although the literature states that alpha therapy is superior to beta therapy [1], there is a total absence of combined alpha and beta therapy for tumor treatment.

This study has developed a nano-formulation of [^{223}Ra] $RaCl_2$ co-loaded with [^{198}Au] Au nanoparticles for bone cancer therapy.

2. Materials and Methods

2.1. Reagents

Phosphate-buffered saline (PBS), PBS/EDTA, bovine serum albumin (BSA), methylated bovine serum albumin (mBSA), Freund's complete adjuvant, Histopaque reagent, Pluronic F127, TRAcP staining kit, DMEM high glucose, fetal bovine serum, M-CSF, RANK-L, doxorubicin, chloroauric acid, tetraoctylammonium bromide, sodium borohydride, Poly-D-lysine, glucose, HEPES, calcium, and magnesium were purchased from Sigma Aldrich (St. Louis, MO, USA).

2.2. Preparation of the Nano-Formulations

2.2.1. [198. Au]AuNPs

Firstly, the non-radioactive AuNPs were synthetized. A gold solution of chloroauric acid ($HAuCl_4 \times 3H_2O$, 0.20 mmol, 78.7 mg) and tetraoctylammonium bromide (TOABr, 0.23 mmol, 126.8 mg) was dissolved in 10 mL of methanol and stirred vigorously for 24 h. Then, sodium borohydride ($NaBH_4$ 2 mmol, 75.6 mg, dissolved in 5 mL of ice water) was added to the mixture, and the solution was kept under stirring for 8 h. After this period, the reaction mixture was ultracentrifuged (40,000 rpm for 30 min) to remove insoluble agglomerates. The supernatant was collected and concentrated by evaporation. The agglomerates were precipitated by adding ethanol to the solution. Then, the precipitate was extracted with minimal amounts of methanol several times. The AuNPs solution was precipitated again by ethanol and finally dried under a vacuum.

Then, the samples of AuNPs were irradiated in the Argonauta reactor (power of 340 W), installed at the Nuclear Engineering Institute (Brazil). The sample was irradiated for 12 h using a thermal neutron flow of 3.2 × 109 $n \cdot cm^{-2} \cdot s^{-1}$, with an average thermal neutron energy of 0.0025 eV.

2.2.2. Radioactivity Measure

The induced activity of the [^{198}Au]AuNPs was determined by a gamma spectrometry system with a hyper pure germanium (HPGe) detector, with a diameter of 6.2 cm, height of 4 cm, active volume of 41.1 cm^3, and detection efficiency of 30%, coupled with the multichannel analyzer (Canberra) with 8192 channels. The detector was surrounded by a lead cover of ~10 cm to reduce the background. The measurement time for each sample was standardized at 3600 s (1 h).

2.3. Detection Efficiency

The detection efficiency for each energy type was determined using a LabSOCS (Laboratory SOurceless Calibration Software, Canberra, Australia). It was necessary to design the geometry used in a computational environment by inserting the physical, chemical, and geometric characteristics of the sample holder used, the detector, and the sample to be analyzed. After entering the data, the software simulates the detection efficiency values for each energy type. Then, the software doubles the number of voxels and repeats the entire process, obeying the convergence criteria and comparing the values until satisfactory convergence is obtained.

2.3.1. Nanomicelles of [^{223}Ra]$RaCl_2$

A mass of 1 mg/mL of [^{223}Ra]$RaCl_2$ was weighed and added to the micellar dispersion of Pluronic F127. The system was gently stirred using a magnetic bar (Magnetic Stirrer, IKA, C-MAG HS-7) for 5 min and then processed for 5 min using an ultrasonic processor (UP100H, Hielscher, power: 100%, cycle: 1) in an ice bath at 10 °C.

2.3.2. Nanomicelles of [^{223}Ra]$RaCl_2$ Co-Loaded with [^{198}Au]AuNPs

A mass of 1 mg/mL of [^{223}Ra]$RaCl_2$ (~3.7 MBq) was weighed and added to the micellar dispersion of Pluronic F127. The system was gently stirred using a magnetic bar (Magnetic Stirrer, IKA, C-MAG HS-7) for 5 min and then processed for 3 min using an ultrasonic processor (UP100H, Hielscher, power: 100%, cycle: 1) in an ice bath at 10 °C. Then, a mass of 500 μg of [^{198}Au]AuNPs (~1.85 MBq) was added and ultrasonicated for more than 2 min using an ultrasonic processor (UP100H, Hielscher, power: 100%, cycle: 1) in an ice bath at 10 °C.

The dispersion of polymeric nanomicelles containing [^{223}Ra]$RaCl_2$ and [^{198}Au]AuNPs was stored in an amber flask for further analysis, in refrigeration (2–8 °C).

2.4. Characterization

2.4.1. Particle Size

The particle size, size distribution, and polydispersity index (PDI) of the [^{198}Au]AuNPs, 127-Pluronic-[^{223}Ra]$RaCl_2$ nanomicelles, and nanomicelles of [^{223}Ra]$RaCl_2$ co-loaded with [^{198}Au]AuNPs were determined by dynamic light scattering (DLS), using Zetasizer Nano ZS (Malvern Instruments, Malvern, UK). Measurements were performed in triplicate at 25 °C, and the laser incidence angle in relation to the sample was 173° using a 12 mm^2 quartz cuvette. The mean ± standard deviation (SD) was assessed.

2.4.2. Atomic Force Microscopy

The AFM analysis was performed using a Multimode 8 microscope (Bruker, Santa Barbara, CA, USA). The following three central characterizations were conducted: [^{198}Au]AuNPs, 127-Pluronic-[^{223}Ra]$RaCl_2$ nanomicelles, and nanomicelles of [^{223}Ra]$RaCl_2$ co-loaded with [^{198}Au]AuNPs. ScanAsyst-Air probes (Bruker, Santa Barbara, CA, USA) were used for these measurements, with a nominal tip ratio of 2 nm and a nominal spring constant of 0.4 N/m. However, the actual spring constant was calibrated by the thermal noise method. A drop of all sample solutions was deposited in freshly cleaved mica. The scanning mode used was PeakForce Tapping Quantitative Nanomechanics (QNM), with a resolution of 256 × 256 lines per scan and a scan frequency of 0.5 Hz.

2.5. In Vitro Cytotoxicity

2.5.1. Cell Culture

The SaOS-2 cells, a human osteosarcoma cell line, were plated in a density of 1×10^4 cells/well for 24h. The cells were maintained in a DMEM/D-glucose (high glucose) medium, supplemented with 10% FBS, penicillin (0.5 U/mL), and streptomycin (0.5 mg/mL). The cells were incubated at 37 °C in a humidified atmosphere of 5% CO_2. The cells were grown to confluence in 75 cm^2 culture flasks and were detached by brief treatment with trypsin (0.1%)/EDTA (0.01%).

2.5.2. Proliferation Assay

The SaOS-2 cells (1×10^4 cells/well) were seeded and allowed to attach for 24 h. The cells were divided into the following three groups: pure [^{223}Ra]$RaCl_2$, 127-Pluronic-[^{223}Ra]$RaCl_2$+[^{198}Au]AuNPs nanomicelles, and 127-Pluronic-[^{223}Ra]$RaCl_2$ nanomicelles, in the following three distinct activities: C1: 37 kBq, C2: 18.5 kBq, and C3: 4.44 kBq. The radioactivity ratio of ^{223}Ra to ^{198}Au in the co-loaded nanomicelles is 8.4. After 24 h, the cells were washed, and the number of attached cells was determined using the MTT assay.

2.5.3. Statistical Analysis

Statistical analysis of the data was performed using the GraphPad Prism 7.3 software (GraphPad Software, San Diego, CA, USA). The differences between the means of the two groups were compared using the one-way ANOVA test and confirmed by the Bonferroni post-test. The results are presented as means ± standard deviation (S.D.). The values of * $p < 0.05$, ** $p < 0.01$, *** $p < 0.005$, and **** $p < 0.0001$ will be considered statistically significant.

3. Results

3.1. Synthesis and Irradiation of Gold Nanoparticles (AuNPs)

Once synthesized, the AuNPs were irradiated under pre-established conditions, and were then able to produce the [^{198}Au]AuNPs. The gamma spectrum obtained with the HPGe detector shows the specific range (412 KeV) of ^{198}Au, as shown in Figure 1.

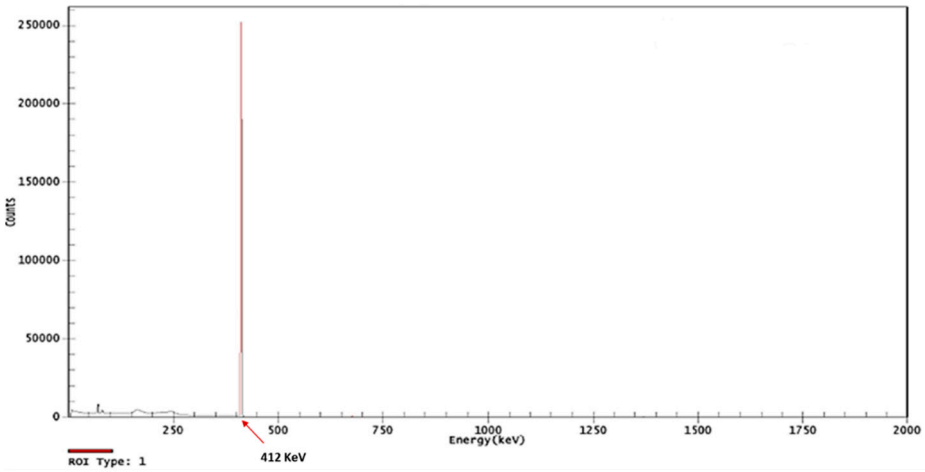

Figure 1. Gamma spectrometry using an HPGe detector from the ^{198}Au, corroborating the efficacy of the irradiation process in forming [^{198}Au]AuNPs.

3.2. Particle Size

The DLS analysis of [^{198}Au]AuNPs showed the formation of very small nanoparticles (13 nm) with very high monodisperse behavior, confirmed by the PDI (0.106) (Figure 2).

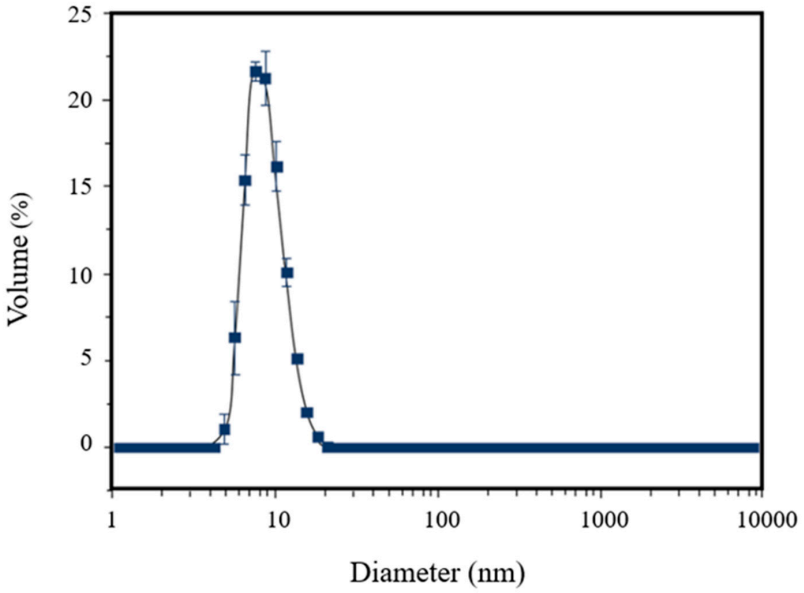

Figure 2. Dynamic light scattering analysis of [^{198}Au]AuNPs, showing a mean size of 13 nm and a PDI of 0.106 (±0.089).

3.3. Atomic Force Microscopy

The morphology of the [^{198}Au]AuNPs was investigated by AFM (Figure 3). Figure 3A shows an AFM height image of a cluster of [^{198}Au] Au nanoparticles. The particles have a homogeneous morphology, with the maximum height on the map reaching 19.7 nm, in regions where the NPs are then superimposed, as evidenced in the three-dimensional image (Figure 3B). The cross section shown in Figure 3C corresponds to the three NPs marked with a dashed light blue line in Figure 3A. The diameters are 14.4 nm, 10.7 nm, and 13.1 nm, considering the horizontal distance taken from the width at the half-height of the particle. These values follow the DLS results.

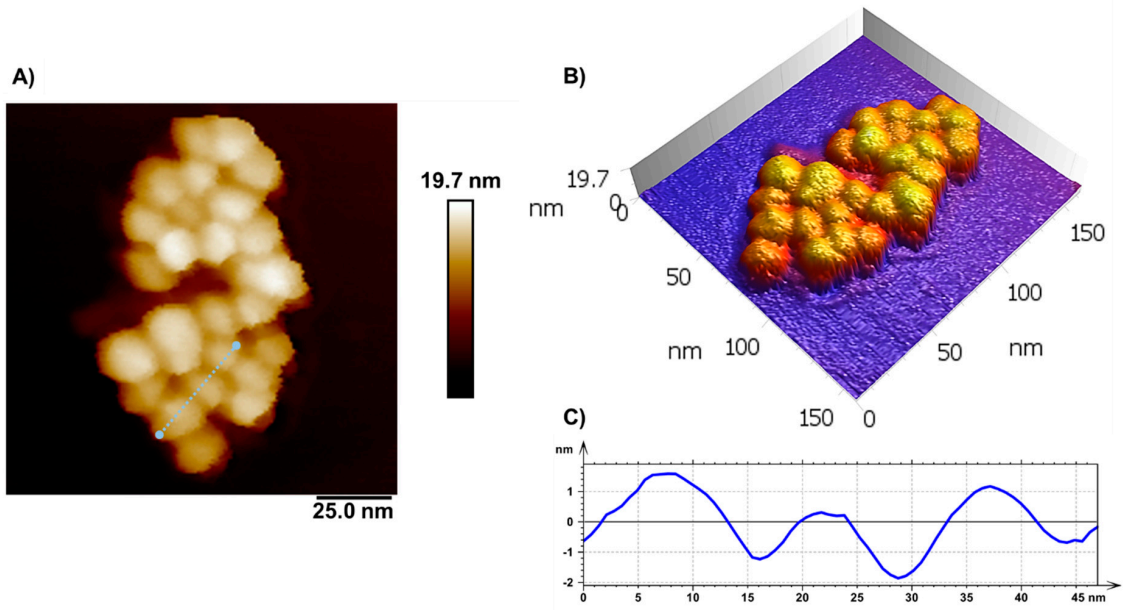

Figure 3. Topographic AFM image of [^{198}Au]AuNPs. (**A**) Heightmap of AuNPs cluster and (**B**) its respective three-dimensional visualization. (**C**) Cross section over the AuNPs in the corresponding region, highlighted in image (**A**) (dotted line in light blue). The particle diameter observed in the AFM measurements is compatible with the values observed in the DLS measurements.

3.4. Nanomicelles of [^{223}Ra] $RaCl_2$

3.4.1. Particle Size

The dynamic light scattering analysis of [^{223}Ra]$RaCl_2$ nanomicelles showed a mean size of 149 nm, with a PDI of 0.0096 (±0.0002), corroborating the monodispersive value (Figure 4).

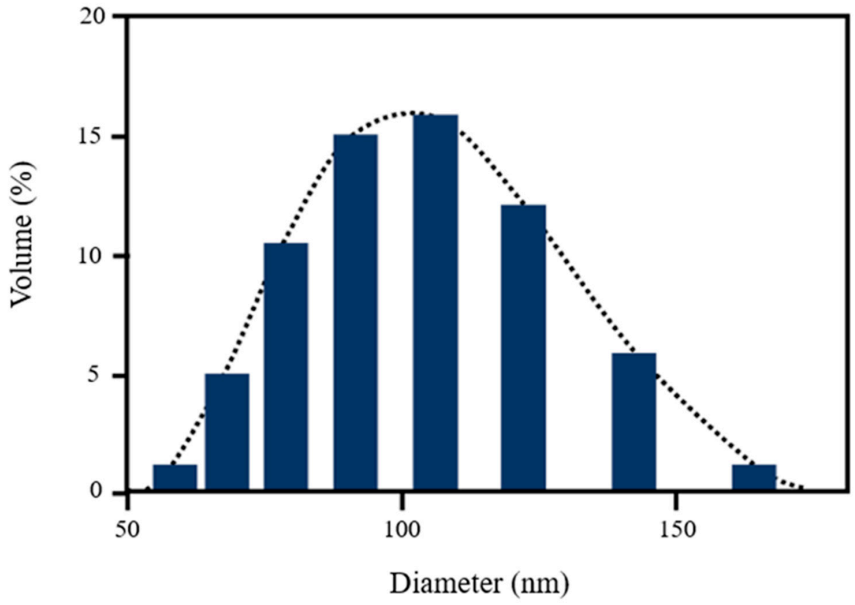

Figure 4. Dynamic light scattering analysis of [^{223}Ra]$RaCl_2$ nanomicelles, showing a mean size of 149 nm and a PDI of 0.0096 (±0.0002).

3.4.2. Nanomicelles of [^{223}Ra]$RaCl_2$ Co-Loaded with [^{198}Au]AuNPs

The DLS analysis of [^{223}Ra]$RaCl_2$ co-loaded with [^{198}Au]AuNPs showed a larger size than the pure [^{223}Ra]$RaCl_2$, due to the incorporation of [^{198}Au]AuNPs. The mean diameter was 296 nm. In addition, it was possible to observe an increase in the PDI value, probably due to the intermicellar destabilization caused by alpha and beta emission, as shown in Figure 5.

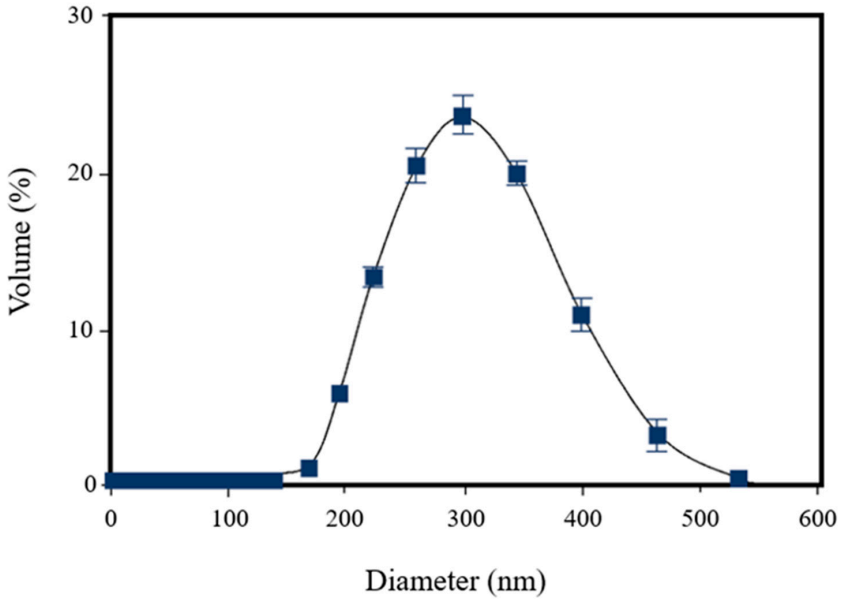

Figure 5. Dynamic light scattering analysis of [^{223}Ra]$RaCl_2$ co-loaded with [^{198}Au]AuNPs, showing a mean size of 296 nm and a PDI of 0.201 (±0.096).

3.5. Atomic Force Microscopy of Nanomicelles Systems

The analyses of the ultrastructure of pure nanomicelles (empty), [^{223}Ra]$RaCl_2$ nanomicelles, and [^{223}Ra]$RaCl_2$ co-loaded with [^{198}Au]AuNPs nanomicelles were performed by AFM, and compared with the 127-Pluronic blank nanomicelles sample (Figure 6). Figure 6A shows a 127-Pluronic white nanomicelles film. Polymeric chain structures, with a diameter of 263.4 ± 12.1 nm, are observed. The maximum film height is 359 nm. The three-dimensional representation of Figure 6 is shown in Figure 6D–F, in which the absence of globular structures is evident.

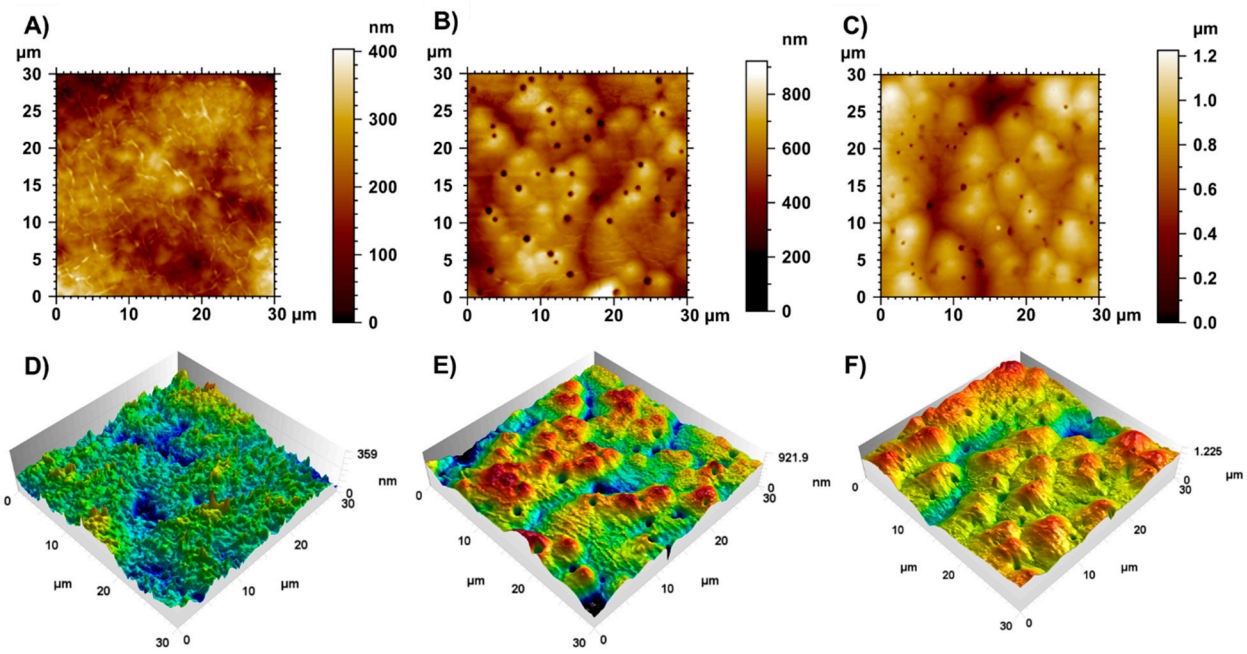

Figure 6. Atomic force microscopy height map of the pure (127-Pluronic) nanomicelles film (**A**), 127-Pluronic-[^{223}Ra]$RaCl_2$ nanomicelles film (**B**), and [^{223}Ra]$RaCl_2$ co-loaded with [^{198}Au]AuNPs film (**C**), and their respective three-dimensional topographies (images (**D**–**F**)). The increase in height scale bar values indicates the filling of the 127-Pluronic nanomicelles with ^{223}Ra and ^{223}Ra + [^{198}Au]AuNPs.

Figure 6C shows the AFM height image of the [^{223}Ra]$RaCl_2$ co-loaded with [^{198}Au]AuNPs film. Once again, it is possible to observe globular structures, with a maximum height of 1.225 µm. Such structures suggest the filling of 127-Pluronic nanomicelles with ^{223}Ra and ^{198}Au. Depressions in the micellar film are also present in this sample (Figure 6F). Since these holes are only observed in the 127-Pluronic-[^{223}Ra] and [^{223}Ra]$RaCl_2$ co-loaded with [^{198}Au]AuNPs films, they can be promoted by emitting alpha and beta particles from the radioactive nanomicelles. However, this emission is not able to destabilize the nanomicelles clusters.

3.6. In Vitro Cytotoxicity

The cytotoxicity effect on human osteosarcoma of the nanosystems developed is expressed in Figure 7. It is possible to observe a very potent effect, mainly in 127-Pluronic-[^{223}Ra]$RaCl_2$+[^{198}Au]AuNPs nanomicelles and 127-Pluronic-[^{223}Ra]$RaCl_2$ nanomicelles, when compared with the pure [^{223}Ra]$RaCl_2$, demonstrating that the combination of alpha and beta therapy increases the cytotoxicity effect.

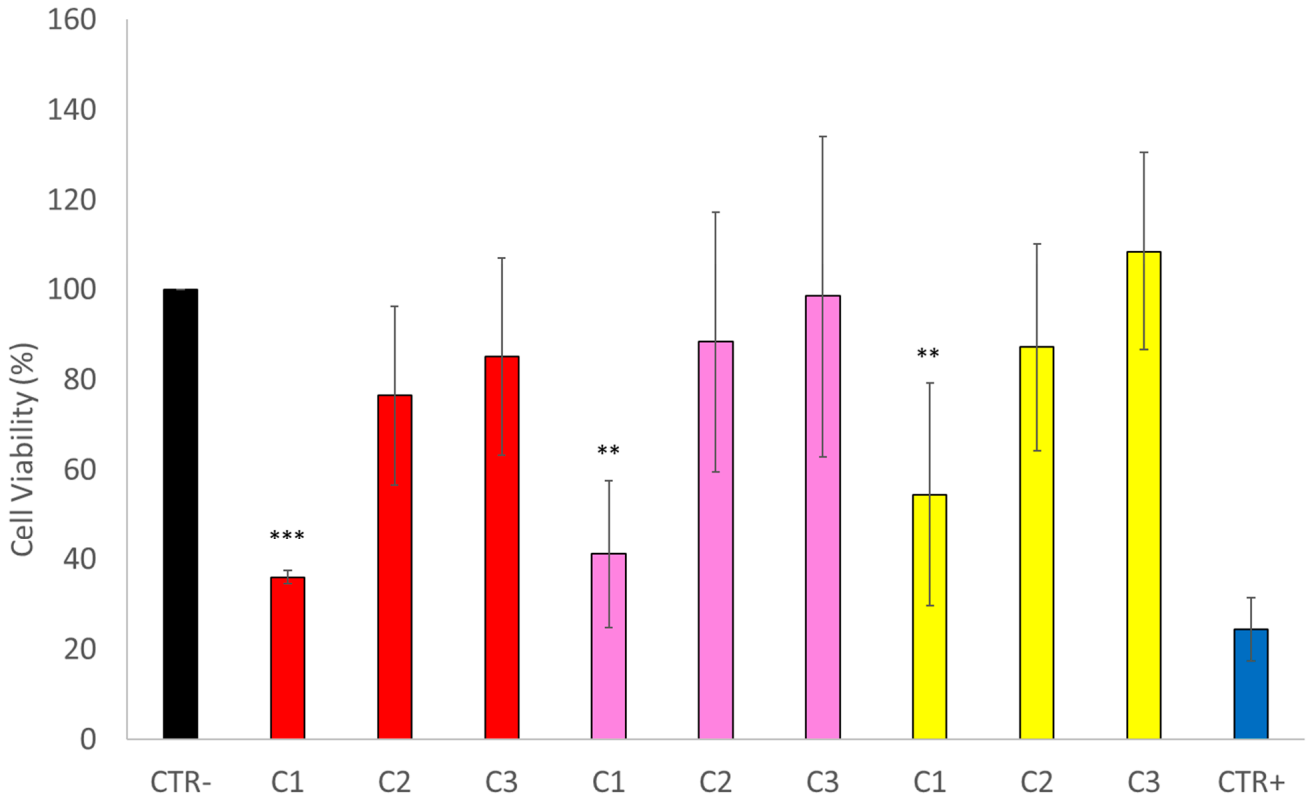

Figure 7. In vitro cytotoxicity results in human osteosarcoma SaOS-2 cells exposed to different nanosystems, using three different activities (C1: 37 kBq, C2: 18.5 kBq, and C3: 4.44 kBq) for each of the following formulations: [^{223}Ra]$RaCl_2$+[^{198}Au]AuNPs nanomicelles (in red), [^{223}Ra]$RaCl_2$ nanomicelles (in pink), and [^{223}Ra]$RaCl_2$ (in yellow). ** $p < 0.01$, *** $p < 0.005$.

4. Discussion

Radionuclide therapy is a safe and effective approach to treat primary cancers, as well as distant metastases. In this sense, beta- or alpha-emitting radionuclides have been primarily used [70]. However, there are a lack of radiopharmaceuticals that deliver simultaneous alpha and beta radiations, which would have remarkable potential for treating tumors. Alpha and beta particles have high energy in different magnitudes; consequently, they have different mean penetration ranges in tissue, for depositing their energies. Hence, alpha-/beta-labeled radiopharmaceuticals would combine the long-range crossfire effect of beta radiation with the DNA localization effect of alpha radiation, among other effects [1]. In addition, successful treatment would be reached using lower doses of alpha and beta emitters.

Therefore, we designed and prepared a novel nanoradiopharmaceutical, containing [^{223}Ra]$RaCl_2$ co-loaded with [^{198}Au]AuNPs into nanomicelles, for radionuclide therapy of bone cancer using alpha and beta radiations simultaneously. Here, to the best of our knowledge, we presented the first findings of combining alpha and beta therapy in the same formulation. In addition, we are the first to report the radiolabeling of nanomicelles with ^{223}Ra for delivering alpha radiation into tumor cells.

To fulfill our goal, the non-radioactive AuNPs were firstly fabricated using chemical synthesis. Through light scattering analysis, the AuNPs obtained a mean size of 13 nm and a PDI value of 0.106 (±0.089). Furthermore, the AFM analyses corroborated the DLS results, confirming the quality and homogeneity of our AuNPs. Then, the AuNPs were activated under neutron irradiation to obtain the [^{198}Au]AuNPs, similar to previous reports [11]. Biodistribution studies (Table S1—Supplemental Information) have shown high liver uptake of [^{198}Au]AuNPs at 2 h and 6 h post-injection in healthy mice. After 24 h

of intravenous injection, the liver uptake decreased, while accumulating in the kidneys, suggesting renal clearance of [^{198}Au]AuNPs.

Following this, the [^{223}Ra]$RaCl_2$ nanomicelles were prepared using a simple and fast method. The DLS analysis of [^{223}Ra]$RaCl_2$ nanomicelles showed a mean size of 149 nm and a PDI of 0.0096 ($\pm$ 0.0002).

Finally, [^{223}Ra]$RaCl_2$ and [^{198}Au]AuNPs were co-loaded into polymeric nanomicelles, and the final dispersion was characterized by DLS and AFM techniques. The DLS analysis revealed a mean size of 296 nm and a PDI value of 0.201 ($\pm$0.096). Moreover, the AFM images showed globular structures and holes because of the emissions of alpha and beta particles. Despite this, these emissions cannot destabilize the formed agglomerates, proving the quality of the nanomicelles.

Next, the in vitro cytotoxicity of these alpha–beta nanomicelles (127-Pluronic-[^{223}Ra]$RaCl_2$+[^{198}Au]AuNPs) was evaluated in human osteosarcoma cells (SaOS-2). It was also compared with the in vitro cytotoxicity of the following two formulations: [^{223}Ra]$RaCl_2$ and 127-Pluronic- [^{223}Ra]$RaCl_2$. The results showed that the three formulations could kill SaOS-2 cells using three activities (37 kBq, 18.5 kBq, and 4.44 kBq). Nevertheless, the 127-Pluronic-[^{223}Ra]$RaCl_2$+[^{198}Au]AuNPs formulation significantly increased cell death as the radioactive activity increased (37 kBq), compared with other activities and formulations. Hence, these findings are very promising. Radionuclide therapy has the advantage of delivering a concentrated dose to target tumor tissues, while preserving the surrounding healthy tissues, unlike the other current cancer therapies [19,39,67,71,72]. For the first time, the simultaneous ability of alpha and beta radiations to kill cancer cells has been demonstrated, using a low radioactive dose and obtaining high efficacy.

5. Conclusions

The combination of alpha and beta radiations in the same nanoprobe would represent a very efficient tool for cancer treatment. Our in vitro findings are the first to demonstrate the remarkable ability of alpha–beta nanoprobes to kill cancer cells using a low radioactive dose. Future works should aim to evaluate the in vivo therapeutic effect and safe use of our nanomicelles of [^{223}Ra]$RaCl_2$ co-loaded with [^{198}Au]AuNPs in bone cancer-bearing mice. Conversely, this work may lead to further studies involving the functionalization of these alpha–beta nanoprobes for targeted radionuclide therapy beyond bone cancer.

Supplementary Materials: The following supporting information can be downloaded at: https://www.mdpi.com/article/10.3390/polym14071405/s1, Table S1: Biodistribution data of [^{198}Au]AuNPs in healthy mice.

Author Contributions: B.N.R.F.S.: software, validation, formal analysis, investigation, data curation, writing—original draft preparation. M.S.O.P.: software, validation, formal analysis, investigation, data curation, writing—original draft preparation. A.O.d.S.d.B.: software, validation, formal analysis, investigation, data curation, writing—original draft preparation. E.R.F.R.R.: software, validation, formal analysis, investigation, data curation, writing—original draft preparation. H.O.K.-H.: software, validation, formal analysis, investigation, data curation, writing—original draft preparation. E.R.-J: Conceptualization, methodology, validation, writing—original draft preparation, writing—review and editing, visualization. J.F.S.D.F.: software, validation, formal analysis, investigation, data curation, writing—original draft preparation, dos Santos. C.C.d.S.: Conceptualization, methodology, validation, writing—original draft preparation, writing—review and editing, visualization. L.M.R.A.: Conceptualization, methodology, software, validation, formal analysis, investigation, resources, data curation, writing—original draft preparation, writing—review and editing, visualization, supervision, project administration, funding acquisition. M.F.A.: Conceptualization, methodology, software, validation, formal analysis, investigation, resources, data curation. S.G.-P.: Conceptualization, methodology, software, validation, formal analysis, investigation, resources, data curation, writing—original draft preparation. R.S.-O.: Conceptualization, methodology, software, validation, formal analysis, investigation, resources, data curation, writing—original draft preparation, writing—review and editing, visualization, supervision, project administration, funding acquisition. All authors have read and agreed to the published version of the manuscript.

Funding: This study was funded by the Carlos Chagas Filho Foundation for Research Support of Rio de Janeiro State (FAPERJ) (Cientista do Nosso Estado: E-26/200.815/2021; Rede NanoSaude: E-26/010.000981/2019; Pesquisa na UEZO: E-26/010.002362/2019; Temáticos: E-26/211.269/2021; Infraestrutura e Pesquisa na UEZO e UERJ: E-26//211.207/2021; Bolsa de Pós Doutorado Senior (PDS): E-26/202.320/2021) CNPq (Bolsa de Produtividade 1B: 301069/2018-2) to Ralph Santos-Oliveira.

Institutional Review Board Statement: This article does not contain any studies with human participants or animals performed by any of the authors.

Informed Consent Statement: Not applicable.

Data Availability Statement: All data will be available under request.

Conflicts of Interest: The authors declare no conflict of interest.

References

1. Marcu, L.; Bezak, E.; Allen, B.J. Global comparison of targeted alpha vs. targeted beta therapy for cancer: In vitro, in vivo and clinical trials. *Crit. Rev. Oncol. Hematol.* **2018**, *123*, 7–20. [CrossRef]
2. Ersahin, D.; Doddamane, I.; Cheng, D. Targeted radionuclide therapy. *Cancers* **2011**, *3*, 3838–3855. [CrossRef] [PubMed]
3. Yeong, C.-H.; Cheng, M.; Ng, K.-H. Therapeutic radionuclides in nuclear medicine: Current and future prospects. *J. Zhejiang Univ. Sci. B* **2014**, *15*, 845. [CrossRef]
4. Welch, M.J.; Hawker, C.J.; Wooley, K.L. The Advantages of Nanoparticles for PET. *J. Nucl. Med.* **2009**, *50*, 1743–1746. [CrossRef] [PubMed]
5. Parveen, K.; Banse, V.; Ledwani, L. Green synthesis of nanoparticles: Their advantages and disadvantages. *AIP Conf. Proc.* **2016**, *1724*, 020048. [CrossRef]
6. Anselmo, A.C.; Mitragotri, S. Nanoparticles in the clinic. *Bioeng. Transl. Med.* **2016**, *1*, 10–29. [CrossRef] [PubMed]
7. Cascella, M.; Rajnik, M.; Aleem, A.; Dulebohn, S.C.; di Napoli, R. *Features, Evaluation, and Treatment of Coronavirus (COVID-19)*; StatPearls Publishing: Treasure Island, FL, USA, 2021.
8. Mudshinge, S.R.; Deore, A.B.; Patil, S.; Bhalgat, C.M. Nanoparticles: Emerging carriers for drug delivery. *Saudi Pharm. J.* **2011**, *19*, 129–141. [CrossRef] [PubMed]
9. Black, K.C.L.; Wang, Y.; Luehmann, H.P.; Cai, X.; Xing, W.; Pang, B.; Zhao, Y.; Cutler, C.S.; Wang, L.V.; Liu, Y.; et al. Radioactive 198Au-doped nanostructures with different shapes for in vivo analyses of their biodistribution, tumor uptake, and intratumoral distribution. *ACS Nano* **2014**, *8*, 4385–4394. [CrossRef] [PubMed]
10. Jeon, J. Review of Therapeutic Applications of Radiolabeled Functional Nanomaterials. *Int. J. Mol. Sci.* **2019**, *20*, 2323. [CrossRef]
11. Xuan, S.; da Silva de Barrosb, A.O.; Nunes, R.C.; Ricci-Junior, E.; Da Silva, A.X.; Sahid, M.; Alencar, L.M.R.; Dos Santos, C.C.; Morandi, V.; Alexis, F.; et al. Radioactive gold nanocluster (198-AuNCs) showed inhibitory effects on cancer cells lines. *Artif. Cells Nanomed. Biotechnol.* **2020**, *48*, 1214–1221. [CrossRef]
12. Pei, P.; Liu, T.; Shen, W.; Liu, Z.; Yang, K. Biomaterial-mediated internal radioisotope therapy. *Mater. Horiz.* **2021**, *8*, 1348–1366. [CrossRef]
13. Katti, K.V.; Kannan, R.; Kattumori, V.; Pandrapraganda, R.; Rahing, V.; Cutler, C.; Boote, E.J.; Casteel, S.W.; Smith, C.J.; Robertson, J.D.; et al. Hybrid gold nanoparticles in molecular imaging and radiotherapy. *Czechoslov. J. Phys.* **2006**, *56*, D23–D34. [CrossRef]
14. Chanda, N.; Kan, P.; Watkinson, L.D.; Shukla, R.; Zambre, A.; Carmack, T.L.; Engelbrecht, H.; Lever, J.R.; Katti, K.; Fent, G.M.; et al. Radioactive gold nanoparticles in cancer therapy: Therapeutic efficacy studies of GA-198AuNP nanoconstruct in prostate tumor–bearing mice. *Nanomed. Nanotechnol. Biol. Med.* **2010**, *6*, 201–209. [CrossRef]
15. de Souza, C.D.; Zeituni, C.A.; Rosero, W.A.A.; Nogueira, B.R.; Rostelato, M.E.C.M. New gold-198 nanoparticle synthesis to be used in cancer treatment. *Braz. J. Radiat. Sci.* **2021**, *9*. [CrossRef]
16. Bai, X.; Wang, Y.; Song, Z.; Feng, Y.; Chen, Y.; Zhang, D.; Lin, F. The Basic Properties of Gold Nanoparticles and their Applications in Tumor Diagnosis and Treatment. *Int. J. Mol. Sci.* **2020**, *21*, 2480. [CrossRef] [PubMed]
17. Siddique, S.; Chow, J.C.L. Gold Nanoparticles for Drug Delivery and Cancer Therapy. *Appl. Sci.* **2020**, *10*, 3824. [CrossRef]
18. Bailly, A.-L.; Correard, F.; Popov, A.; Tselikov, G.; Chaspoul, F.; Appay, R.; Al-Kattan, A.; Kabashin, A.V.; Braguer, D.; Esteve, M.-A. In vivo evaluation of safety, biodistribution and pharmacokinetics of laser-synthesized gold nanoparticles. *Sci. Rep.* **2019**, *9*, 12890. [CrossRef] [PubMed]
19. Peng, J.; Liang, X. Progress in research on gold nanoparticles in cancer management. *Medicine* **2019**, *98*, e15311. [CrossRef]
20. Singh, P.; Pandit, S.; Mokkapati, V.R.S.S.; Garg, A.; Ravikumar, V.; Mijakovic, I. Gold Nanoparticles in Diagnostics and Therapeutics for Human Cancer. *Int. J. Mol. Sci.* **2018**, *19*, 1979. [CrossRef] [PubMed]
21. Dykman, L.A.; Khlebtsov, N.G. Immunological properties of gold nanoparticles. *Chem. Sci.* **2017**, *8*, 1719–1735. [CrossRef]
22. Graczyk, A.; Pawlowska, R.; Jedrzejczyk, D.; Chworos, A. Gold Nanoparticles in Conjunction with Nucleic Acids as a Modern Molecular System for Cellular Delivery. *Molecules* **2020**, *25*, 204. [CrossRef] [PubMed]
23. Rodriguez-Quijada, C.; Sánchez-Purrà, M.; de Puig, H.; Hamad-Schifferli, K. Physical Properties of Biomolecules at the Nanomaterial Interface. *J. Phys. Chem. B* **2018**, *122*, 2827–2840. [CrossRef]

24. Zhang, X. Gold Nanoparticles: Recent Advances in the Biomedical Applications. *Cell Biochem. Biophys.* **2015**, *72*, 771–775. [CrossRef] [PubMed]
25. Lopez-Chaves, C.; Soto-Alvaredo, J.; Montes-Bayon, M.; Bettmer, J.; Llopis, J.; Sanchez-Gonzalez, C. Gold nanoparticles: Distribution, bioaccumulation and toxicity. In vitro and in vivo studies. *Nanomedicine* **2018**, *14*, 1–12. [CrossRef]
26. Singh, P.; Ahn, S.; Kang, J.-P.; Veronika, S.; Huo, Y.; Singh, H.; Chokkaligam, M.; Farh, M.E.-A.; Aceituno, V.C.; Kim, Y.J.; et al. In vitro anti-inflammatory activity of spherical silver nanoparticles and monodisperse hexagonal gold nanoparticles by fruit extract of Prunus serrulata: A green synthetic approach. *Artif. Cells Nanomed. Biotechnol.* **2018**, *46*, 2022–2032. [CrossRef] [PubMed]
27. Choi, B.J.; Jung, K.O.; Graves, E.E.; Pratx, G. A gold nanoparticle system for the enhancement of radiotherapy and simultaneous monitoring of reactive-oxygen-species formation. *Nanotechnology* **2018**, *29*, 504001. [CrossRef] [PubMed]
28. Azharuddin, M.; Zhu, G.H.; Das, D.; Ozgur, E.; Uzun, L.; Turner, A.P.F.; Patra, H.K. A repertoire of biomedical applications of noble metal nanoparticles. *Chem. Commun.* **2019**, *55*, 6964–6996. [CrossRef]
29. Kang, M.S.; Lee, S.Y.; Kim, K.S.; Han, D.-W. State of the Art Biocompatible Gold Nanoparticles for Cancer Theragnosis. *Pharmaceutics* **2020**, *12*, 701. [CrossRef] [PubMed]
30. Santos, V.F.; Nicolucci, P. Dose Enhancement Factor in Radiation Therapy With Nanoparticles: A Monte Carlo-Simulation Study. *Rev. Bras. Física Méd.* **2017**, *11*, 2–6. Available online: https://www.rbfm.org.br/rbfm/article/view/426/v11n3p2-6 (accessed on 22 October 2021).
31. Kong, F.Y.; Zhang, J.W.; Li, R.F.; Wang, Z.X.; Wang, W.J.; Wang, W. Unique Roles of Gold Nanoparticles in Drug Delivery, Targeting and Imaging Applications. *Molecules* **2017**, *22*, 1445. [CrossRef]
32. Shen, W.; Zhou, H.; Liu, T.; Pei, P.; Huang, J.; Yi, X.; Yang, K. The potential clinical applications of radionuclide labeled/doped gold-based nanomaterials. *Radiat. Med. Prot.* **2020**, *1*, 186–195. [CrossRef]
33. Faivre, S.; Rimassa, L.; Finn, R.S. Molecular therapies for HCC: Looking outside the box. *J. Hepatol.* **2020**, *72*, 342–352. [CrossRef]
34. Al-Yasiri, A.Y.; White, N.E.; Katti, K.V.; Loyalka, S.K. Estimation of tumor and local tissue dose in gold nanoparticles radiotherapy for prostate cancer. *Rep. Pract. Oncol. Radiother.* **2019**, *24*, 288–293. [CrossRef]
35. Cholkar, K.; Hirani, N.D.; Natarajan, C. Nanotechnology-Based Medical and Biomedical Imaging for Diagnostics. In *Emerging Nanotechnologies for Diagnostics, Drug Delivery and Medical Devices*; Elsevier: Amsterdam, The Netherlands, 2017; pp. 355–374. [CrossRef]
36. Shukla, R.; Chanda, N.; Zambre, A.; Upendran, A.; Katti, K.; Kulkarni, R.R.; Nune, S.K.; Casteel, S.W.; Smith, C.J.; Vimal, J.; et al. Laminin receptor specific therapeutic gold nanoparticles (198AuNP-EGCg) show efficacy in treating prostate cancer. *Proc. Natl. Acad. Sci. USA* **2012**, *109*, 12426–12431. [CrossRef]
37. Katti, K.V.; Khoobchandani, M.; Thipe, V.; Al_Yasiri, A.; Loyalka, S.K.; Sakr, T.; Lugão, A.B. Prostate tumor therapy advances in nuclear medicine: Green nanotechnology toward the design of tumor specific radioactive gold nanoparticles. *J. Radioanal. Nucl. Chem.* **2018**, *318*, 1737–1747. [CrossRef]
38. Al-Yasiri, A.Y.; Khoobchandani, M.; Cutler, C.S.; Watkinson, L.; Carmack, T.; Smith, C.J.; Kuchuk, M.; Loyalka, S.K.; Lugão, A.B.; Katti, K.V. Mangiferin functionalized radioactive gold nanoparticles (MGF-198AuNPs) in prostate tumor therapy: Green nanotechnology for production, in vivo tumor retention and evaluation of therapeutic efficacy. *Dalt. Trans.* **2017**, *46*, 14561–14571. [CrossRef]
39. Sgouros, G. α-Particle–Emitter Radiopharmaceutical Therapy: Resistance Is Futile. *Cancer Res.* **2019**, *79*, 5479–5481. [CrossRef] [PubMed]
40. Rovais, M.R.A.; Alirezapour, B.; Moassesi, M.E.; Amiri, M.; Novin, F.B.; Maadi, E. Internalization capabilities of gold-198 nanoparticles: Comparative evaluation of effects of chitosan agent on cellular uptake into MCF-7. *Appl. Radiat. Isot.* **2018**, *142*, 85–91. [CrossRef] [PubMed]
41. Dekempeneer, Y.; Keyaerts, M.; Krasniqi, A.; Puttemans, J.; Muyldermans, S.; Lahoutte, T.; D'Huyvetter, M.; Devoogdt, N. Targeted alpha therapy using short-lived alpha-particles and the promise of nanobodies as targeting vehicle. *Expert Opin. Biol. Ther.* **2016**, *16*, 1035–1047. [CrossRef] [PubMed]
42. Pouget, J.; Constanzo, J. Revisiting the Radiobiology of Targeted Alpha Therapy. *Front. Med.* **2021**, *8*, 692436. [CrossRef]
43. Kim, Y.S.; Brechbiel, M.W. An overview of targeted alpha therapy. *Tumour Biol.* **2012**, *33*, 573–590. [CrossRef]
44. Liberal, F.D.C.G.; O'Sullivan, J.M.; McMahon, S.J.; Prise, K.M. Targeted Alpha Therapy: Current Clinical Applications. *Cancer Biother. Radiopharm.* **2020**, *35*, 404–417. [CrossRef] [PubMed]
45. Yoon, S.M.; Chu, F.-I.; Ruan, D.; Steinberg, M.L.; Raldow, A.; Lee, P. Assessment of Toxic Effects Associated With Dose-Fractionated Radiotherapy Among Patients With Cancer and Comorbid Collagen Vascular Disease. *JAMA Netw. Open* **2021**, *4*, e2034074. [CrossRef] [PubMed]
46. Dauer, L.T.; Williamson, M.J.; Humm, J.; O'Donoghue, J.; Ghani, R.; Awadallah, R.; Carrasquillo, J.; Pandit-Taskar, N.; Aksnes, A.-K.; Biggin, C.; et al. Radiation Safety Considerations For The Use Of 223RaCl2 De In Men With Castration-Resistant Prostate Cancer. *Health Phys.* **2014**, *106*, 494. [CrossRef] [PubMed]
47. Morris, M.J.; Corey, E.; Guise, T.A.; Gulley, J.L.; Kelly, W.K.; Quinn, D.I.; Scholz, A.; Sgouros, G. Radium-223 mechanism of action: Implications for use in treatment combinations. *Nat. Rev. Urol.* **2019**, *16*, 745–756. [CrossRef] [PubMed]
48. BGarashchenko, L.; Korsakova, V.A.; Yakovlev, R.Y. Radiopharmaceuticals Based on Alpha Emitters: Preparation, Properties, and Application. *Phys. At. Nucl.* **2019**, *81*, 1515–1525. [CrossRef]

49. Bauckneht, M.; Rebuzzi, S.; Signori, A.; Donegani, M.; Murianni, V.; Miceli, A.; Borea, R.; Raffa, S.; Damassi, A.; Ponzano, M.; et al. The Prognostic Role of Baseline Metabolic Tumor Burden and Systemic Inflammation Biomarkers in Metastatic Castration-Resistant Prostate Cancer Patients Treated with Radium-223: A Proof of Concept Study. *Cancers* **2020**, *12*, 3213. [CrossRef]
50. van der Zande, K.; Oyen, W.J.G.; Zwart, W.; Bergman, A.M. Radium-223 Treatment of Patients with Metastatic Castration Resistant Prostate Cancer: Biomarkers for Stratification and Response Evaluation. *Cancers* **2021**, *17*, 4346. [CrossRef]
51. Trujillo-Nolasco, M.; Morales-Avila, E.; Cruz-Nova, P.; Katti, K.V.; Ocampo-García, B. Nanoradiopharmaceuticals Based on Alpha Emitters: Recent Developments for Medical Applications. *Pharmaceutics* **2021**, *13*, 1123. [CrossRef]
52. Datta, P.; Ray, S. Nanoparticulate formulations of radiopharmaceuticals: Strategy to improve targeting and biodistribution properties. *J. Label. Compd. Radiopharm.* **2020**, *63*, 333–355. [CrossRef]
53. Mokhodoeva, O.; Vlk, M.; Málková, E.; Kukleva, E.; Mičolová, P.; Štamberg, K.; Slouf, M.; Dzhenloda, R.; Kozempel, J. Study of 223Ra uptake mechanism by Fe_3O_4 nanoparticles: Towards new prospective theranostic SPIONs. *J. Nanoparticle Res.* **2016**, *18*, 301. [CrossRef]
54. Vasiliev, A.N.; Severin, A.; Lapshina, E.; Chernykh, E.; Ermolaev, S.; Kalmykov, S. Hydroxyapatite particles as carriers for 223Ra. *J. Radioanal. Nucl. Chem.* **2016**, *311*, 1503–1509. [CrossRef]
55. Cholkar, K.; Patel, A.; Vadlapudi, A.D.; Mitra, A.K. Novel Nanomicellar Formulation Approaches for Anterior and Posterior Segment Ocular Drug Delivery. *Recent Pat. Nanomed.* **2012**, *2*, 82–95. [CrossRef] [PubMed]
56. Atanase, L.I.; Desbrieres, J.; Riess, G. Micellization of synthetic and polysaccharides-based graft copolymers in aqueous media. *Prog. Polym. Sci.* **2017**, *73*, 32–60. [CrossRef]
57. Tawfik, S.M.; Azizov, S.; Elmasry, M.R.; Sharipov, M.; Lee, Y.I. Recent Advances in Nanomicelles Delivery Systems. *Nanomater* **2020**, *11*, 70. [CrossRef]
58. Trinh, H.M.; Joseph, M.; Cholkar, K.; Mitra, R.; Mitra, A.K. Nanomicelles in Diagnosis and Drug Delivery. In *Emerging Nanotechnologies for Diagnostics, Drug Delivery and Medical Devices*; Elsevier: Amsterdam, The Netherlands, 2017; pp. 45–58. [CrossRef]
59. Hruby, M.; Konak, C.; Kucka, J.; Vetrik, M.; Filippov, S.K.; Vetvicka, D.; Mackova, H.; Karlsson, G.; Edwards, K.; Rihova, B.; et al. Thermoresponsive, hydrolytically degradable polymer micelles intended for radionuclide delivery. *Macromol. Biosci.* **2009**, *9*, 1016–1027. [CrossRef] [PubMed]
60. Hara, E.; Makino, A.; Kurihara, K.; Ueda, M.; Hara, I.; Kawabe, T.; Yamamoto, F.; Ozeki, E.; Togashi, K.; Kimura, S. Radionuclide therapy using nanoparticle of 131I-Lactosome in combination with percutaneous ethanol injection therapy. *J. Nanoparticle Res.* **2013**, *15*, 2131. [CrossRef]
61. Yang, Y.; Alencar, L.M.R.; Pijeira, M.S.O.; Batista, B.D.S.; França, A.R.S.; Rates, E.R.D.; Lima, R.C.; Gemini-Piperni, S.; Santos-Oliveira, R. [223Ra] $RaCl_2$ nanomicelles showed potent effect against osteosarcoma: Targeted alpha therapy in the nanotechnology era. *Drug Deliv.* **2022**, *29*, 186–191. [CrossRef] [PubMed]
62. Kancharla, S.; Zoyhofski, N.A.; Bufalini, L.; Chatelais, B.F.; Alexandridis, P. Association between nonionic amphiphilic polymer and ionic surfactant in aqueous solutions: Effect of polymer hydrophobicity and micellization. *Polymers* **2020**, *12*, 1831. [CrossRef] [PubMed]
63. Managa, M.; Britton, J.; Amuhaya, E.K.; Nyokong, T. Photophysical properties of GaCl 5, 10, 15, 20-tetra (1-pyrenyl) porphyrinato incorporated into Pluronic F127 micelle. *J. Lumin.* **2017**, *185*, 34–41. [CrossRef]
64. Oh, K.S.; Song, J.Y.; Cho, S.H.; Lee, B.S.; Kim, S.Y.; Kim, K.; Jeon, H.; Kwon, I.C.; Yuk, S.H. aclitaxel-loaded Pluronic nanoparticles formed by a temperature-induced phase transition for cancer therapy. *J. Control. Release* **2010**, *148*, 344–350. [CrossRef] [PubMed]
65. Torchilin, V.P. Structure and design of polymeric surfactant-based drug delivery systems. *J. Control. Release* **2001**, *73*, 137–172. [CrossRef]
66. Gong, J.; Chen, M.; Zheng, Y.; Wang, S.; Wang, Y. Polymeric micelles drug delivery system in oncology. *J. Control. Release* **2012**, *159*, 312–323. [CrossRef] [PubMed]
67. Wu, S.; Helal-Neto, E.; dos Santos Matosc, A.P.; Jafari, A.; Kozempel, J.; de Albuquerque Silvaf, Y.J.; Serrano-Larrea, C.; Junior, S.A.; Ricci-Junior, E.; Alexis, F.; et al. Radioactive polymeric nanoparticles for biomedical application. *Drug Deliv.* **2020**, *27*, 1544–1561. [CrossRef]
68. Beik, J.; Khateri, M.; Khosravi, Z.; Kamrava, S.K.; Kooranifar, S.; Ghaznavi, H.; Shakeri-Zadeh, A. Gold nanoparticles in combinatorial cancer therapy strategies. *Coord. Chem. Rev.* **2019**, *387*, 299–324. [CrossRef]
69. Toro, M.C.G.; Schlegel, J.; Giraldo, C.H.C. Direct Synthesis of Radioactive Gold Nanoparticles Using a Research Nuclear Reactor. *J. Nucl. Med. Technol.* **2018**, *46*, 280–284. [CrossRef] [PubMed]
70. Sgouros, G.; Bodei, L.; McDevitt, M.R.; Nedrow, J.R. Radiopharmaceutical therapy in cancer: Clinical advances and challenges. *Nat. Rev. Drug Discov.* **2020**, *19*, 589–608. [CrossRef] [PubMed]
71. Güleç, B.A.; Yurt, F. Treatment with Radiopharmaceuticals and Radionuclides in Breast Cancer: Current Options. *Eur. J. Breast Health* **2021**, *17*, 214. [CrossRef] [PubMed]
72. de Barros, A.B.; Tsourkas, A.; Saboury, B.; Cardoso, V.N.; Alavi, A. Emerging role of radiolabeled nanoparticles as an effective diagnostic technique. *EJNMMI Res.* **2012**, *2*, 39. [CrossRef] [PubMed]